THE JOURNAL OF PHYSICAL CHEMISTRY Letters

Letter

pubs.acs.org/JPCL

CO Oxidation at the Interface of Au Nanoclusters and the Stepped-CeO_2(111) Surface by the Mars–van Krevelen Mechanism

Hyun You Kim*,† and Graeme Henkelman*

Department of Chemistry and Biochemistry, University of Texas at Austin, Austin, Texas 78712-0165, United States

Supporting Information

ABSTRACT: DFT+U calculations of CO oxidation by Au_{12} nanoclusters supported on a stepped-CeO_2(111) surface show that lattice oxygen at the step edge oxidizes CO bound to Au NCs by the Mars–van Krevelen (M-vK) mechanism. We found that CO_2 desorption determines the rate of CO oxidation, and the vacancy formation energy is a reactivity descriptor for CO oxidation. Our results suggest that the M-vK mechanism contributes significantly to CO oxidation activity at Au particles supported on the nano- or meso-structured CeO_2 found in industrial catalysts.

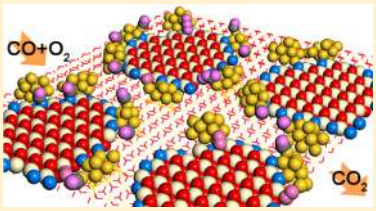

SECTION: Surfaces, Interfaces, Porous Materials, and Catalysis

Cerium oxide is a promising candidate for advanced heterogeneous catalysis as well as a prevalent supporting material for catalysis at supported Au nanoparticles (NPs).[1,2] The unique properties of CeO_2 have been recognized as a combination of high oxygen storage and release capacity, facile oxygen vacancy formation, and the presence of a sharp Ce *f*-band.[1,2] Experimental studies have shown that the surface of CeO_2 can be enriched with oxygen vacancies and that metal NPs or nanoclusters (NCs) bind strongly to these vacancies.[3−5] Moreover, the step edges on CeO_2 surfaces have also been recognized as a binding site of metal NPs/NCs.[4]

The oxidation chemistry of CeO_2 supported Au NPs/NCs (Au/CeO_2) has been extensively studied, and especially the reactive species.[6−10] The critical role of the interface between the supporting oxide and the supported metal NPs/NCs has been highlighted by experimental and theoretical studies in several systems.[6−18] Rodriguez and co-workers have shown that the Au supported CeO_2 inverse-catalyst has a high activity for water–gas shift reaction compared to the conventional Au/CeO_2 catalyst.[11] Zhou et al. showed a clear relationship between the length of the Au-CeO_2 interface and the CO oxidation reactivity on the Au/CeO_2 multilayers.[19] The Neurock and Yates groups showed that the Au–TiO_2 interface activates the following reactions: CO oxidation,[12] partial oxidation of acetic acid,[20] and low-temperature H_2 oxidation.[21] Very recently, Bruix et al. reported that lattice oxygen of a (Ce–Ti)O_2 mixed oxide can directly participate in the water–gas shift reaction by supported Pt NCs.[14]

Another interesting feature of CeO_2-supported metal NPs/NCs is the nanosize effect of the CeO_2 support on the catalytic activity. Several recent reports on the nanosize effect of CeO_2 support on the catalytic activity of supported metal NPs/NCs confirm the relevancy of the metal–CeO_2 interface to the oxidation catalysis.[7,8,13] Guzman et al. reported experimental results showing that the nanosized CeO_2 increases the CO oxidation activity by supported Au and that the CeO_2 support supplies the reactive oxygen species directly to the supported Au NPs.[8] The Neyman and Illas groups reported a lower vacancy formation energy (E_{vac}) of nanosized CeO_2, and showed that the reactive oxygen atoms are supplied by oxygen spillover from the CeO_2 to supported Pt NPs.[13]

In our previous studies, we have suggested that O_2 bound to the Au–Ce^{3+} interface oxidizes CO bound to Au NCs.[10] We also found that lattice oxygen from the CeO_2 surface can be directly used as an oxygen source for CO oxidation at the Au–CeO_2 interface by cation doping.[9] From an industrial perspective, however, a model system of Au NPs/NCs supported on a flat defect-free CeO_2 surface is not particularly relevant. Au NPs/NCs supported on rough polycrystalline surfaces, oxide NPs, or meso-structures such as zeolites would be more appropriate models for industrial-grade catalysts.

In this Letter, we are taking a step toward modeling real catalysts by studying the mechanism of CO oxidation by Au_{12} NCs supported on stepped-CeO_2, using density functional theory (DFT). We are focusing on the role of the interface between the supporting CeO_2 and the supported Au NCs via previously reported interface-mediated CO oxidation mechanisms: oxygen spillover from the CeO_2 to the Au NPs;[8] CO oxidation by the O_2 bound to the Au–Ce^{3+} interface;[10] and CO oxidation by the Mars–van Krevelen (M-vK) mechanism.[9] We find that the low E_{vac} of the stepped-CeO_2 support promotes CO oxidation at the Au–CeO_2 interface by the M-vK mechanism. The experimentally reported CeO_2 NP/Au inverse catalyst[11] was also studied to confirm our computational results. Our findings provide insight into the oxidation catalysis by Au/CeO_2 catalysts and the origin of their catalytic activity.

Nilius et al. have resolved the morphology of steps in the CeO_2(111) surface and reported three different structures: two types of ⟨110⟩ steps and one ⟨211⟩ step.[22] They confirmed that the simulated STM images of these DFT-interpreted steps were

Received: November 2, 2012
Accepted: December 22, 2012

   dx.doi.org/10.1021/jz301778b | *J. Phys. Chem. Lett.* 2013, 4, 216–221

in close agreement with experimental STM data. We reproduced these three types of steps on the $CeO_2(111)$ surface (CeO_2-step) (refer to Figure 1 for the detailed morphology). The CeO_2-U and CeO_2-D ($\langle 110\rangle$-type steps) were produced by adding a 2/5 ML of three atomic layers of CeO_2 (a $Ce_{10}O_{20}$ wire) on a 5×5 $CeO_2(111)$ slab with six atomic layers. The CeO_2-M ($\langle 211\rangle$-type step) was constructed by adding a 3/8 ML of three atomic layers of CeO_2 (a Ce_9O_{18} wire) on a $4 \times 3\sqrt{3}$ of $CeO_2(111)$ slab with six atomic layers. The edge atoms along one side of a partial CeO_2 ad-layer was used to model CO oxidation at a CeO_2-step. Differences in E_{vac} between our systems and thicker models (total 12 atomic layers) are smaller than 30 meV, demonstrating convergence with respect to system size. A Au NC comprised of 12 atoms was optimized at the step edge of each CeO_2-step to generate the Au/CeO_2-step models (see Figure 2a,b,c). Three lowest atomic layers of CeO_2 were fixed during optimizations. The structure of Au_{12} NC was adapted from our previously reported Au_{13} NC.[9,10] One corner Au atom was removed from the side of Au_{13} NC to produce a better Au-CeO_2-step interface structure. Detailed information on the stability of our Au NC and the selection of the CeO_2 support can be found in our previous studies.[9,10]

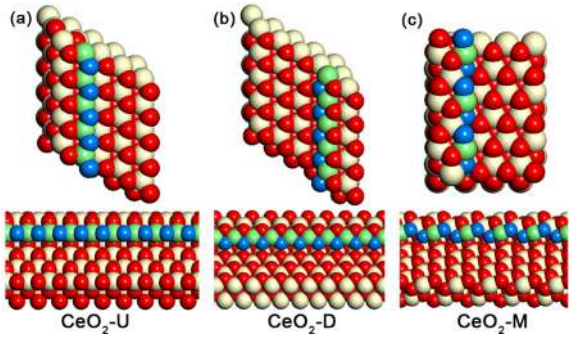

Figure 1. Three kinds of steps on the $CeO_2(111)$ surface used for the current study. CeO_2-U (a) and CeO_2-D (b) describe the $\langle 110\rangle$ type steps with upper and lower rows of oxygen atoms, respectively. CeO_2-M (c) describes the $\langle 211\rangle$-type step with mixed type of edge oxygen atoms. Ivory and red spheres represent Ce and O atoms, respectively. Ce and O atoms along the step edge are colored in green and blue, respectively.

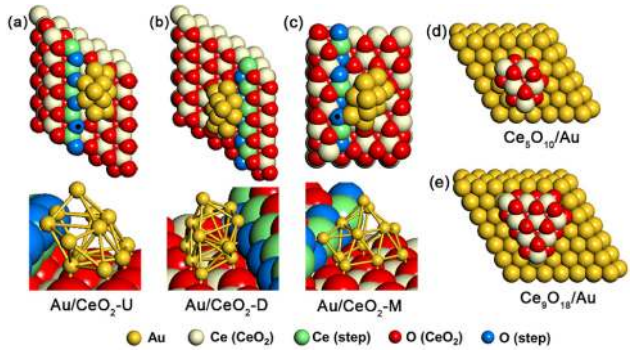

Figure 2. Morphology of studied catalyst models: (a–c) Au/CeO_2-step and (d,e) CeO_2/Au. Black dots represent the location of edge oxygen atoms that were tested for M-vK mechanism of CO oxidation.

We performed spin-polarized DFT calculations with the VASP code[23] and the PBE[24] functional. In order to treat the highly localized Ce 4*f*-orbital, DFT+U[25] with U_{eff} = 5 eV was applied.[9,10] The interaction between the ionic core and the valence electrons was described by the projector augmented wave method,[26] and the valence electrons with a plane wave basis up to an energy cutoff was 400 eV. The Brillouin zone was sampled at the Γ-point. The convergence criteria for the electronic structure and the geometry were 10^{-4} eV and 0.01 eV/Å, respectively. We used the Gaussian smearing method with a finite temperature width of 0.1 eV in order to improve convergence of states near the Fermi level. The location and energy of transition states (TSs) were calculated with the climbing-image nudged elastic band method.[27,28] E_{vac}, the energy required to remove an oxygen atom from the CeO_2-step, was calculated with reference to the energy of gas phase O_2.

A comparison of E_{vac} between the reference 5×5, nine-layer $CeO_2(111)$ slab and three CeO_2-step structures (CeO_2-U, CeO_2-D, and CeO_2-M) shows that oxygen atoms at the step edge are weakly bound to the CeO_2 matrix (Table 1). This is natural due to the lower coordination of these oxygen atoms. Considering previously reported low E_{vac} of CeO_2 nanocrystallites[29] and their enhancing effect on the catalytic activity of supported Pt NPs,[13] the CeO_2-step is also expected to promote CO oxidation by the Au/CeO_2-step. The E_{vac} of three CeO_2-step structures lie between 1.5 and 1.7 eV, which is consistent with literature values.[29] These E_{vac} values also fall near the previously suggested maximum E_{vac} for the activation of the M-vK mechanism of CO oxidation by Au NC supported on doped-CeO_2.[9] The E_{vac} of the second vacancy at the first nearest neighboring position from the first vacancy (Table 1) shows that the vacancy pairing is a rare event in CeO_2-U and CeO_2-D steps, whereas the divacancy can be occasionally found at the step edge of the CeO_2-M.

Figure 2 shows three different optimized initial Au/CeO_2-step models. Low-coordinated surface sites on the CeO_2 surface, such as at step edges or surface vacancies, are regarded as strong binding sites for metal (Au or Ag) NPs.[4,10] We found that the CeO_2-step strongly binds Au NCs, making it a preferential binding site of supported Au NPs/NCs (Table S1). The binding energy of a Au NC on the CeO_2-U and CeO_2-M

Table 1. E_{vac} Calculated in CeO_2-step and Au/CeO_2-step[a]

	CeO_2-STO[b]	CeO_2-U	CeO_2-D	CeO_2-M	Au/CeO_2-U	Au/CeO_2-M
E_{vac} (eV)	2.48	1.66 (2.07)	1.62 (2.17)	1.52 (1.62)	1.75	1.02

[a]Values in parentheses represent the E_{vac} of the second vacancy. E_{vac} of two Au/CeO_2-step systems where the M-vK mechanism of CO oxidation was tested are presented. [b]Adopted from ref 9.

dx.doi.org/10.1021/jz301778b | J. Phys. Chem. Lett. 2013, 4, 216–221

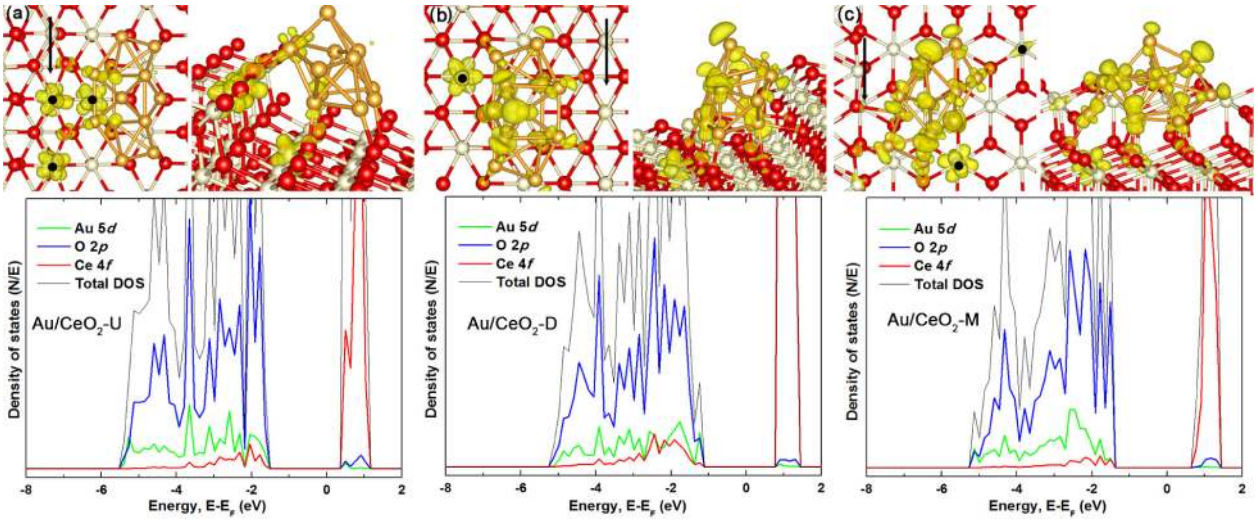

Figure 3. Density plots of the two highest occupied Kohn−Sham molecular orbitals associated with the introduction of Au NP on CeO_2-step: (a) CeO_2-U, (b) CeO_2-D, and (c) CeO_2-M. Corresponding total and partial density of states are presented below. Black dots represent the location of reduced Ce^{3+} ions upon supporting of Au NP. Black arrow represents the step edge. Yellow, ivory, and red spheres represent Au, Ce, and O atoms, respectively. Density of states was calculated with a 4 × 4 × 1 K-points grid (10 irreducible K-points). Hybridization between O-2*p* and Au-5*d* orbitals are responsible for the strong Au-CeO_2-step interaction. O-2*p*, Au-5*d*, and Ce-4*f* orbitals are contributing to the frontier orbitals.

steps was even stronger than that on the stoichiometric CeO_2 and partially reduced CeO_2 surfaces with a divacancy (Table S1). Stronger Au binding on CeO_2-step confirms the previously reported binding tendency of Au NPs on polycrystalline CeO_2 substrate; Au NPs prefer the step edge.[4]

The location of the frontier orbitals (the sum of the charge densities of two highest lying Kohn−Sham molecular orbitals) of Au/CeO_2-U, Au/CeO_2-D, and Au/CeO_2-M and their density of states, presented in Figure 3, show that Au binding at the CeO_2-step is through Au−O bonds (hybridization of Au-*d* and O-*p* orbitals). Reduced Ce^{3+} ions are located at the neighboring sites to the Au−O bonds composing the highest occupied molecular orbital (HOMO).

CO oxidation at the Au-CeO_2-step interface was studied considering three mechanisms: the M-vK mechanism of CO oxidation[9] (oxidation of Au−CO* by an oxygen atom at the step edge), the oxygen spillover mechanism[8,13] (oxidation of Au-CO* by an oxygen atom spontaneous transferred from the step edge to the Au NC), and CO oxidation by O_2 bound to the Au−Ce^{3+} interface.[10]

In the case of Au/CeO_2-step structures, the spillover of lattice oxygen of the CeO_2 step was not found to be energetically favorable. The binding energy of atomic oxygen on the Au NP is −0.5 eV, which is close to the experimental binding energy estimated by Campbell's group for tiny Au particles on TiO_2(110) (−0.85 eV),[30] requiring more than 1.0 eV for oxygen transfer. We also have examined the oxygen spillover mechanism on Au NCs supported on stoichiometric CeO_2,[10] partially reduced CeO_2,[10] and doped-CeO_2[9] and found that oxygen spillover is energetically prohibited in these systems as well. We postulate, therefore, that this mechanism, which requires either a low E_{vac} of CeO_2 support or strong binding of atomic oxygen on Au NPs/NCs, is a special case for Au NPs/NCs supported on small CeO_2 nanocrystallites or NPs, for example, the truncated-octahedral $Ce_{80}O_{160}$ NP reported by Neyman and co-workers[29] where the E_{vac} is as low as 0.46 eV (PW91+U calculation). As reported by Neyman and co-workers, CO oxidation by CeO_2-supported strong oxo-phillic NPs such as Pt NPs would favor the oxygen spillover mechanism.[13]

In the case of Au/CeO_2−U where two Ce^{4+} ions at the step edge are reduced (Figure 3a), we examined whether these Au−Ce^{3+} interface binds a gas phase O_2 and activates CO oxidation by O_2 bound to the Au−Ce^{3+} interface. The calculated binding energy of gas phase O_2 at the Au−Ce^{3+} interface is as low as −0.36 eV. Because the entropic contribution to the Gibbs free energy of O_2 desorption at the conventional operating temperature of CO oxidation (−0.64 eV at 298 K and 1 bar; the standard entropy of O_2 at 298 K is 205.14 J mol^{-1} K^{-1}; see Supporting Information)[31,32] is greater than the binding energy, O_2 coverage at the Au−Ce^{3+} interface would be lower than that of Au-CO*.[10] Presumably, reduced Ce^{3+} ions and low coordinated oxygen atoms at the step edge stabilize each other in the form of local Ce_2O_3 clusters, thus, reduced Ce^{3+} ions are reluctant to bind additional gas phase O_2.

The next step of CO oxidation by O_2 at the Au−Ce^{3+} interface takes place on the surface of the Au NC.[10] Since the activation energy is 0.08 eV at the interface of the Au NC and the reduced CeO_2(111)),[10] we postulate a low barrier in the case of our Au/CeO_2-step as well. In such a case, the relative coverage of CO and O_2 at the interface would account for the preferred reaction mechanism. Because CO adsorption is 3 times stronger than that of O_2, the M-vK mechanism would be favored for CO oxidation by the weakly bound O_2 molecule at the Au−Ce^{3+} interface. In other cases, where the reduced Ce^{3+} ion is located at the terrace of the CeO_2(111) support (Figure 3), we found that the Au−Ce^{3+} interface does not bind O_2 strongly, which is consistent with what we have reported in Au NCs supported on doped-CeO_2.[9] Likely, the presence of reduced Ce^{3+} is not a sufficient condition for strong O_2 binding at the Au−Ce^{3+} interface. We hypothesize that the binding of O_2 at the Au−Ce^{3+} interface[10] is a result of the systematic attribution of the Ce^{3+} ion adjacent $Au^{\delta-}$ or low coordinated Au atom.

O_2 binding at the Au−Ce^{3+} interface was also examined in Au NCs supported on a partially reduced CeO_2-step with one or two vacancies. We found that O_2 prefers to fill the vacancy

dx.doi.org/10.1021/jz301778b | J. Phys. Chem. Lett. 2013, 4, 216−221

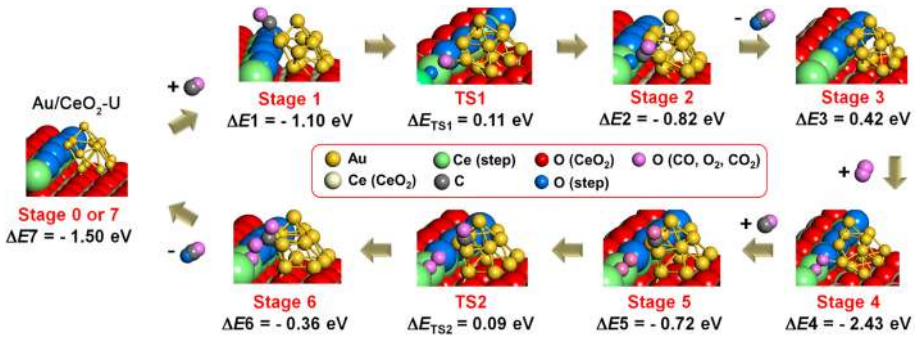

Figure 4. Energetics and the morphology of reaction intermediates of CO oxidation by Au/CeO_2−U. ΔEx is the energy of the x^{th} state relative to that of the previous stage; for example, $\Delta E2$ is the energy difference between stage 2 and stage 1. ΔE_{TSx} is the energy of the x^{th} TS relative to the previous stage (energy barrier of the x^{th} TRI formation).

rather than binding at the Au−Ce^{3+} interface. O_2 bound to the vacancy will oxidize CO by the second-half of the M-vK mechanism.

CO oxidation by the M-vK mechanism was studied in the Au/CeO_2-M and Au/CeO_2-U systems, where CO bound to Au NC (Au−CO*) is in close contact with one of lattice oxygen atoms at the CeO_2-step. The CO oxidation pathway shown in Figure 4 (Au/CeO_2-U) is a typical M-vK mechanism of CO oxidation that we have reported for a Au NC supported on CeO_2 surfaces; CO binding on Au NC (Au-CO*), formation of a triangular reaction intermediate (TRI), CO_2 desorption and vacancy formation, vacancy healing by a gas phase O_2 molecule (V−O_2*), and further oxidation of Au−CO* by a protruding oxygen atom of V−O_2*.[9] The low barrier for TRI formation confirms that the desorption of the first CO_2, which accompanies vacancy formation at the CeO_2-step, is the rate-determining step of CO oxidation by the M-vK mechanism. In both cases, the energy of CO_2 desorption can be supplied by the entropic contribution to the Gibbs free energy of CO_2 desorption (−0.66 eV at 298 K and 1 bar; the standard entropy of CO_2 at 298 K is 213.79 J mol^{-1} K^{-1}),[31,32] suggesting that CO_2 production would not impede the reaction (see Supporting Information).[9] Experimentally observed apparent activation energies for CO oxidation by Au−CeO_2 catalysts are in the vicinity of 0.3 to 0.5 eV, depending on the size of Au NCs and the dimension of CeO_2.[33−35] The energy of CO_2 desorption ($\Delta E3$ = 0.42 eV, Figure 4) is consistent with these experimental findings.

Previously, we have reported that the energy of CO_2 desorption from the first TRI of Au NCs supported on a doped-CeO_2 surface is a function of the E_{vac} of Au/doped-CeO_2.[9] Two additional data points from the Au/CeO_2-U and Au/CeO_2-M (see Supporting Information, Table S2, for energetics of CO oxidation by Au/CeO_2-M) were added to Figure 5. These two data points lie on the red line, which is parallel to the previously reported trend line of the Au/CeO_2 surface. The shift in the data points is likely the result of the size effect in CeO_2, and it shows that the CeO_2-step is a more favorable and volatile oxide support than the flat CeO_2 surface for CO oxidation by the supported Au NPs. The maximum E_{vac} for the activation of the M-vK mechanism of CO oxidation at the interface of Au/CeO_2-step is calculated as 2.10 eV, which is higher than that of the Au/CeO_2 surface (1.58 eV) by 0.52 eV; the Au/CeO_2-step whose E_{vac} is lower than 2.10 eV would be eligible for the spontaneous CO_2 production from the first TRI (see Supporting Information for details). It is not clear yet whether data from other CeO_2 nanostructures, for example

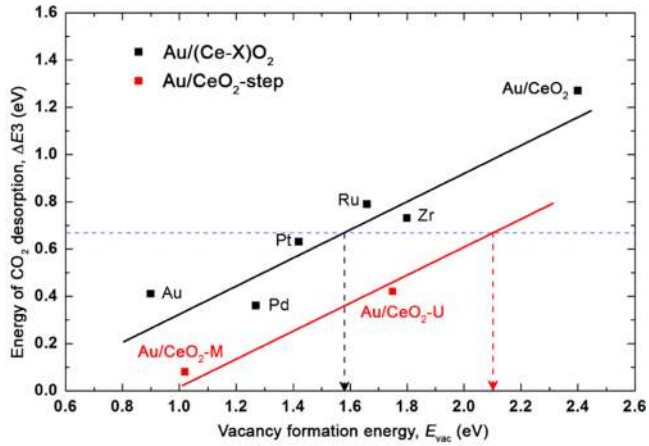

Figure 5. A linear relation is found between E_{vac} and the energy of CO_2 desorption (ΔE_3 as defined in Figure 4) over Au NCs supported on CeO_2-step supports, Au/CeO_2-step, (red data), and doped CeO_2 surfaces, Au/(Ce−X)O_2 (X = Au, Pd, Pt, Ru, or Zr) (black data). Data points of Au/(Ce−X)O_2 were adopted from ref 9. The blue dashed line represents the boundary where ΔE_3 can be overcome by the entropic contribution to the Gibbs free energy of CO_2 desorption, which is −0.66 eV at 298 K. The black and red dashed lines represent the maximum E_{vac} for the activation of the M-vK mechanism of CO oxidation by Au/(Ce−X)O_2 (1.58 eV) and Au/CeO_2-step (2.10 eV), respectively.

CeO_2 NPs or curved steps, will fall on the current trend line (red line in Figure 5). Further investigations would provide a comprehensive picture of how the dimension of nanostructured CeO_2 affects their oxidation potential. We speculate that, as shown in Figure 5, a specific morphology of the CeO_2 nanostructure with a lower E_{vac} would be more favorable for oxidation catalysis by the M-vK mechanism.

Rodriguez and co-workers have reported the excellent catalytic activity of CeO_2/metal inverse catalyst, and their results are recognized as a good example of the critical role of the metal−oxide interface on the oxidation catalysis.[11,36] To examine the oxidation potential of oxygen atoms in a CeO_2 island supported on a metal surface, we constructed CeO_2/Au(111) models (see Figure 2d,e) and calculated the E_{vac} of oxygen atoms of the CeO_2 island at the Au−CeO_2 interface. The E_{vac} of the Ce_5O_9/Au(111) model depends on the location of oxygen atoms varying between 0.95 to 1.32 eV (Table S3). Of course, CeO_2/Au(111) inverse-catalysts could activate CO oxidation by a different mechanism. However, the average E_{vac} of interfacial oxygen atoms (1.19 eV, which is lower than the

dx.doi.org/10.1021/jz301778b | J. Phys. Chem. Lett. 2013, 4, 216−221

threshold E_{vac} (2.10 eV) for the activation of the M-vK mechanism of CO oxidation derived from CeO_2-steps) predicts the strong oxidation potential of these oxygen atoms. The calculated E_{vac} of the larger CeO_2 island, Ce_9O_{18}/Au(111), was increased from that of the Ce_5O_{10}/Au(111) (average E_{vac} = 1.62 eV, see Table S3), predicting that the E_{vac} of the supported CeO_2 of the CeO_2/Au inverse catalyst is highly sensitive to the shape and size, suggesting that the dimension of CeO_2 islands would affect their catalytic activity. We found that Ce atoms in Ce_5O_{10}/Au(111) were reduced as the CeO_2 island acquired extra electron density from Au supports (see Table S4). We will address the size effect of CeO_2 islands on the oxidation catalysis and the detailed mechanism of oxidation catalysis.

Herein, we study various kinds of CO oxidation mechanisms at the interface of the Au NCs supported on the CeO_2-step and find that Au−CO* can be directly oxidized by the protruded oxygen atoms of the CeO_2-step by the M-vK mechanism of oxidation. CO oxidation by the M-vK mechanism at the interface between the CeO_2 support and supported Au NPs/NCs is highly beneficial for the consistency in the catalytic activity because the Au NPs/NCs and CeO_2 are playing different roles without competing for the same binding site; Au and CeO_2 supplies CO and oxygen, respectively. The low activation energy and CO_2 production energy of the Au/CeO_2-step give rise to the high CO oxidation activity of the Au/CeO_2-step, and the E_{vac} is a reactivity descriptor. The maximum E_{vac} that insures spontaneous CO_2 production is higher for the Au/CeO_2-step than that for the Au/CeO_2-surface, suggesting that the CeO_2-step is a better supporting material than the CeO_2-surface for CO oxidation by the Au/CeO_2. Our results also suggest that for CO oxidation by Au NCs supported on nano- or meso-structured CeO_2, which is the case of industrial catalysts, the M-vK mechanism accounts for a large portion of the total activity.

Our previous study and recent report by Bruix et al.[14] shows that doping the CeO_2 surface[9] or making a mixed $(Ce-X)O_2$ oxide[14] would query the participation of lattice oxygen atoms of CeO_2 surface in CO oxidation at the interface between CeO_2 surface and supported metal NPs/NCs. Moreover, current results show that the catalytic activity of the CeO_2-metal NPs/NCs interface can be modified by the dimension of the CeO_2 support. We suggest that combining chemical and morphological optimization of the oxide support is a promising way to extensively modify the activity of oxidation catalysis by supported Au NPs/NCs.

■ ASSOCIATED CONTENT

Supporting Information

Additional data is presented in Tables S1, S2, S3, and S4, and Figures S1 and S2. This material is available free of charge via the Internet at http://pubs.acs.org.

■ AUTHOR INFORMATION

Corresponding Author

*E-mail: hykim8083@gmail.com (H.Y.K.); henkelman@cm.utexas.edu (G.H.). TEL: (512) 471-4179; FAX: (512) 471-6835.

Present Address

[†]Center for Functional Nanomaterials, Brookhaven National Laboratory, Upton, New York, 11973.

Notes

The authors declare no competing financial interest.

■ ACKNOWLEDGMENTS

This work is supported by the Department of Energy under contract DE-SC0001091. All calculations were done at the National Energy Research Scientific Computing Center and the Texas Advanced Computing Center.

■ REFERENCES

(1) Sun, C.; Li, H.; Chen, L. Nanostructured Ceria-Based Materials: Synthesis, Properties, and Applications. *Enery. Environ. Sci.* **2012**, *5*, 8475−8505.

(2) Zhang, C. J.; Michaelides, A.; Jenkins, S. J. Theory of Gold on Ceria. *Phys. Chem. Chem. Phys.* **2010**, *13*, 22−33.

(3) Esch, F.; Fabris, S.; Zhou, L.; Montini, T.; Africh, C.; Fornasiero, P.; Comelli, G.; Rosei, R. Electron Localization Determines Defect Formation on Ceria Substrates. *Science* **2005**, *309*, 752−755.

(4) Baron, M.; Bondarchuk, O.; Stacchiola, D.; Shaikhutdinov, S.; Freund, H. J. Interaction of Gold with Cerium Oxide Supports: CeO_2(111) Thin Films vs CeO_x Nanoparticles. *J. Phys. Chem. C* **2009**, *113*, 6042−6049.

(5) Farmer, J. A.; Campbell, C. T. Ceria Maintains Smaller Metal Catalyst Particles by Strong Metal-Support Bonding. *Science* **2010**, *329*, 933−936.

(6) Camellone, M. F.; Fabris, S. Reaction Mechanisms for the CO Oxidation on Au/CeO_2 Catalysts: Activity of Substitutional Au^{3+}/Au^+ Cations and Deactivation of Supported Au^+ Adatoms. *J. Am. Chem. Soc.* **2009**, *131*, 10473−10483.

(7) Carrettin, S.; Concepcion, P.; Corma, A.; Nieto, J. M. L.; Puntes, V. F. Nanocrystalline CeO_2 Increases the Activity of Au for CO Oxidation by Two Orders of Magnitude. *Angew. Chem., Int. Ed.* **2004**, *43*, 2538−2540.

(8) Guzman, J.; Carrettin, S.; Corma, A. Spectroscopic Evidence for the Supply of Reactive Oxygen during CO Oxidation Catalyzed by Gold Supported on Nanocrystalline CeO_2. *J. Am. Chem. Soc.* **2005**, *127*, 3286−3287.

(9) Kim, H. Y.; Henkelman, G. CO Oxidation at the Interface between Doped CeO_2 and Supported Au Nanoclusters. *J. Phys. Chem. Lett.* **2012**, *3*, 2194−2199.

(10) Kim, H. Y.; Lee, H. M.; Henkelman, G. CO Oxidation Mechanism on CeO_2-Supported Au Nanoparticles. *J. Am. Chem. Soc.* **2012**, *134*, 1560−1570.

(11) Rodriguez, J. A.; Ma, S.; Liu, P.; Hrbek, J.; Evans, J.; Perez, M. Activity of CeO_x and TiO_x Nanoparticles Grown on Au(111) in the Water−Gas Shift Reaction. *Science* **2007**, *318*, 1757−1760.

(12) Green, I. X.; Tang, W. J.; Neurock, M.; Yates, J. T. Spectroscopic Observation of Dual Catalytic Sites During Oxidation of CO on a Au/TiO_2 Catalyst. *Science* **2011**, *333*, 736−739.

(13) Vayssilov, G. N.; Lykhach, Y.; Migani, A.; Staudt, T.; Petrova, G. P.; Tsud, N.; Skala, T.; Bruix, A.; Illas, F.; Prince, K. C.; Matolin, V.; Neyman, K. M.; Libuda, J. Support Nanostructure Boosts Oxygen Transfer to Catalytically Active Platinum Nanoparticles. *Nat. Mater.* **2011**, *10*, 310−315.

(14) Bruix, A.; Rodriguez, J. A.; Ramirez, P. J.; Senanayake, S. D.; Evans, J.; Park, J. B.; Stacchiola, D.; Liu, P.; Hrbek, J.; Illas, F. A New Type of Strong Metal−Support Interaction and the Production of H_2 through the Transformation of Water on Pt/CeO_2(111) and Pt/CeO_x/TiO_2(110) Catalysts. *J. Am. Chem. Soc.* **2012**, *134*, 8968−8974.

(15) Nie, X.; Qian, H.; Ge, Q.; Xu, H.; Jin, R. CO Oxidation Catalyzed by Oxide-Supported $Au_{25}(SR)_{18}$ Nanoclusters and Identification of Perimeter Sites as Active Centers. *ACS Nano* **2012**, *6*, 6014−6022.

(16) López-Haro, M.; Cíes, J. M.; Trasobares, S.; Pérez-Omil, J. A.; Delgado, J. J.; Bernal, S.; Bayle-Guillemaud, P.; Stéphan, O.; Yoshida, K.; Boyes, E. D.; Gai, P. L.; Calvino, J. J. Imaging Nanostructural Modifications Induced by Electronic Metal−Support Interaction Effects at Au||Cerium-Based Oxide Nanointerfaces. *ACS Nano* **2012**, *6*, 6812−6820.

(17) Park, J. B.; Graciani, J.; Evans, J.; Stacchiola, D.; Senanayake, S. D.; Barrio, L.; Liu, P.; Sanz, J. F.; Hrbek, J.; Rodriguez, J. A. Gold,

Copper, and Platinum Nanoparticles Dispersed on $CeO_x/TiO_2(110)$ Surfaces: High Water-Gas Shift Activity and the Nature of the Mixed-Metal Oxide at the Nanometer Level. *J. Am. Chem. Soc.* **2010**, *132*, 356−363.
(18) Stamatakis, M.; Christiansen, M. A.; Vlachos, D. G.; Mpourmpakis, G. Multiscale Modeling Reveals Poisoning Mechanisms of MgO-Supported Au Clusters in CO Oxidation. *Nano Lett.* **2012**, *12*, 3621−3626.
(19) Zhou, Z.; Kooi, S.; Flytzani-Stephanopoulos, M.; Saltsburg, H. The Role of the Interface in CO Oxidation on Au/CeO_2 Multilayer Nanotowers. *Adv. Funct. Mater.* **2008**, *18*, 2801−2807.
(20) Green, I. X.; Tang, W.; Neurock, M.; Yates, J. T. Localized Partial Oxidation of Acetic Acid at the Dual Perimeter Sites of the Au/TiO_2 Catalyst—Formation of Gold Ketenylidene. *J. Am. Chem. Soc.* **2012**, *134*, 13569−13572.
(21) Green, I. X.; Tang, W. J.; Neurock, M.; Yates, J. T. Low-Temperature Catalytic H_2 Oxidation over Au Nanoparticle/TiO_2 Dual Perimeter Sites. *Angew. Chem., Int. Ed.* **2011**, *50*, 10186−10189.
(22) Nilius, N.; Kozlov, S. M.; Jerratsch, J. F.; Baron, M.; Shao, X.; Vines, F.; Shaikhutdinov, S.; Neyman, K. M.; Freund, H. J. Formation of One-Dimensional Electronic States along the Step Edges of $CeO_2(111)$. *ACS Nano* **2012**, *6*, 1126−1133.
(23) Kresse, G.; Furthmuller, J. Efficient Iterative Schemes for Ab Initio Total-Energy Calculations Using a Plane-Wave Basis Set. *Phys. Rev. B* **1996**, *54*, 11169−11186.
(24) Perdew, J. P.; Burke, K.; Ernzerhof, M. Generalized Gradient Approximation Made Simple. *Phys. Rev. Lett.* **1996**, *77*, 3865−3868.
(25) Dudarev, S. L.; Botton, G. A.; Savrasov, S. Y.; Humphreys, C. J.; Sutton, A. P. Electron-Energy-Loss Spectra and the Structural Stability of Nickel Oxide: An LSDA+U Study. *Phys. Rev. B* **1998**, *57*, 1505−1509.
(26) Blochl, P. E. Projector Augmented-Wave Method. *Phys. Rev. B* **1994**, *50*, 17953−17979.
(27) Henkelman, G.; Jonsson, H. Improved Tangent Estimate in the Nudged Elastic Band Method for Finding Minimum Energy Paths and Saddle Points. *J. Chem. Phys.* **2000**, *113*, 9978−9985.
(28) Henkelman, G.; Uberuaga, B. P.; Jonsson, H. A Climbing Image Nudged Elastic Band Method for Finding Saddle Points and Minimum Energy Paths. *J. Chem. Phys.* **2000**, *113*, 9901−9904.
(29) Migani, A.; Vayssilov, G. N.; Bromley, S. T.; Illas, F.; Neyman, K. M. Greatly Facilitated Oxygen Vacancy Formation in Ceria Nanocrystallites. *Chem. Commun.* **2010**, *46*, 5936−5938.
(30) Campbell, C. T.; Sharp, J. C.; Yao, Y. X.; Karp, E. M.; Silbaugh, T. L. Insights into Catalysis by Gold Nanoparticles and Their Support Effects through Surface Science Studies of Model Catalysts. *Faraday Discuss.* **2011**, *152*, 227−239.
(31) Atkins, P.; Paula, J. D. *Physical Chemistry*, 8th ed.; Oxford University Press: New York, 2006.
(32) Metiu, H. *Physical Chemistry: Statistical Mechanics*, 1st ed.; Tayler & Francis: New York, 2006.
(33) Aguilar-Guerrero, V.; Gates, B. C. Kinetics of CO Oxidation Catalyzed by Highly Dispersed CeO_2-Supported Gold. *J. Catal.* **2008**, *260*, 351−357.
(34) Zhou, Z.; Flytzani-Stephanopoulos, M.; Saltsburg, H. Decoration with Ceria Nanoparticles Activates Inert Gold Island/Film Surfaces for the CO Oxidation Reaction. *J. Catal.* **2011**, *280*, 255−263.
(35) Moreau, F.; Bond, G. C. CO Oxidation Activity of Gold Catalysts Supported on Various Oxides and Their Improvement by Inclusion of an Iron Component. *Catal. Today* **2006**, *114*, 362−368.
(36) Rodriguez, J. A.; Graciani, J.; Evans, J.; Park, J. B.; Yang, F.; Stacchiola, D.; Senanayake, S. D.; Ma, S. G.; Perez, M.; Liu, P.; Sanz, J. F.; Hrbek, J. Water−Gas Shift Reaction on a Highly Active Inverse $CeO_x/Cu(111)$ Catalyst: Unique Role of Ceria Nanoparticles. *Angew. Chem., Int. Ed.* **2009**, *48*, 8047−8050.